Iron Contamination in Silicon Wafers Measured with the Pulsed MOS Capacitor Generation Lifetime Technique

Suat-Eng Tan, Dieter K. Schroder, *Life Fellow, IEEE*, Motohiro Kohno, and Morimasa Miyazaki

***Abstract*—The pulsed MOS capacitor generation lifetime technique is used to determine the iron density in boron-doped silicon wafers. Effective generation lifetimes ($\tau_{g,\mathrm{eff}}$) are extracted from the Zerbst plots obtained from the measured capacitance-time (C-t) data. Upon thermal heating at 200 °C for 5 minutes and quenching to 23 °C, iron–boron (Fe–B) pairs dissociate into interstitial iron (Fe_i) and substitutional boron (B). The post-heated $\tau_{g,\mathrm{eff}}$ decreases immediately after heating. As time elapses (pairing time t_p increases) after Fe–B dissociation, $\tau_{g,\mathrm{eff}}$ increases because Fe_i reforms into Fe–B pairs. It takes about four times the time constant (i.e., $t_p \approx 4\tau$) of Fe–B pairing reaction before the post-heated $\tau_{g,\mathrm{eff}}$ recovers to the pre-heated $\tau_{g,\mathrm{eff}}$. An expression is developed to determine the iron density. The iron density obtained from this expression shows good agreement with that measured by deep-level transient spectroscopy.**

***Index Terms*—Impurities, MOS capacitors, semiconductors, semicondutctor device measurements, semiconductor materials, silicon.**

I. Introduction

IRON (Fe) is one of the most prevalent heavy metal impurities in silicon wafers [1]. Its existence leads to yield and reliability problems in integrated circuits [2]. A number of methods are capable of detecting the Fe density. Ion-beam techniques, such as secondary ion mass spectrometry (SIMS) and Rutherford backscattering (RBS), can be used to detect Fe. However, these measurements have Fe detection limits of 5×10^{13} cm^{-3} [3]. Although detection of Fe as low as 10^{11} cm^{-3} is possible by electrical or spectroscopic techniques like deep level transient spectroscopy (DLTS) and electron paramagnetic resonance (EPR) [3], these methods require long measuring times. Both recombination lifetime (τ_r) and diffusion length (L_n) techniques, like microwave photoconductance decay (μPCD) [4], [5] and surface photovoltage (SPV) [6] techniques, are effective in determining the Fe density in silicon. They are fast, noncontact and nondestructive. However, these methods sample a volume over a distance of L_n (typically tens to hundreds of microns). This makes them poorly suited to characterize thin layers, such as epitaxial layers, denuded zones and silicon-on-insulator (SOI) wafers.

What other technique can detect iron density in a simple, rapid and room temperature measurement without having the aforementioned limitations? It turns out that the pulsed MOS capacitor generation lifetime (τ_g) technique is suitable and is addressed here. This technique is very sensitive to interface states at the Si/SiO_2 interface and to impurities in the space-charge region (scr) under the gate. It samples a well-defined volume of materials near the surface, determined by the scr width (typically a micron or less) and the gate area. Carrier generation volume in the scr can be well-controlled by the applied gate voltage. This makes the τ_g technique particularly suited for measurements in thin layers.

II. Experiments

A. Pulsed MOS Capacitor Technique

A popular version of the pulsed MOS capacitor technique was proposed by Zerbst [7]. This technique measures the generation lifetime based on the transient response of a MOS capacitor pulsed into deep depletion. Subsequent refinements were implemented by Schroder [8]–[10] with the consideration of five distinctive thermal generation mechanisms, as illustrated in Fig. 1:

1) bulk space-charge region (scr) generation characterized by the generation lifetime τ_g;
2) lateral surface scr generation characterized by the surface generation velocity s_g;
3) surface scr generation under the gate characterized by the surface generation velocity s_g';
4) quasineutral bulk generation characterized by the minority carrier diffusion length L_n;
5) back surface generation characterized by the generation velocity s_c.

Electron-hole pair generation in the scr is dominant when the device is pulsed at room temperature. Quasineutral bulk generation and diffusion of carriers to the scr dominate for measurements at elevated temperature.

Manuscript received February 7, 2000; revisedMay 12, 2000. This work was supported in part by the Silicon Wafer Engineering and Defect Science Consortium (SiWEDS) (Intel, Komatsu Electronic Metals, MEMC Electronic Materials, Mitsubishi Silicon, Nippon Steel, Okmetic, Sumitomo Sitix Silicon, Texas Instruments, and Wacker Siltronic Corp.). The review of this paper was arranged by Editor J. N. Hollenhorst.

S.-E. Tan was with the Department of Electrical Engineering, Arizona State University, Tempe, AZ 85287 USA. She is now with Wafertech, Camas, WA USA

D. K. Schroder is with the Center for Solid State Electronics Research, Department of Electrical Engineering, Arizona State University, Tempe, AZ 85287 USA.

M. Kohno is with the Development Department, Dainippon Screen Manufacturing Co., Ltd., Kyoto 612, Japan.

M. Miyazaki is with the Research and Development Center, Sumitomo Metal Industries, Ltd, Saga 849-05, Japan.

Publisher Item Identifier S 0018-9383(00)10406-X.

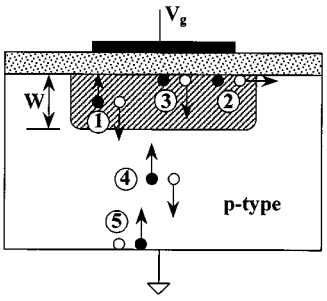

Fig. 1. Space-charge region and quasineutral bulk thermal generation mechanisms of a pulsed MOS capacitor.

The thermal generation rate (G) of the various mechanisms in Fig. 1 is the negative of the change in inversion charge density (dQ_n/dt), given as [11]

$$\begin{aligned} G &= -\frac{dQ_n}{dt} \\ &= G_{(1)} + G_{(2)} + G_{(3)} + G_{(4+5)} \\ &= \frac{qn_iW}{\tau_g} + \frac{qn_is_gA_S}{A_G} + qn_is_{g'} + \frac{qn_i^2D_n}{N_AL_n'} \end{aligned} \tag{1}$$

where

$A_G = \pi r^2$	gate area (r the gate radius);
$A_S = 2\pi rW$	area of the lateral scr (for simplicity assuming the lateral scr width is identical to the vertical scr width W);
L_n'	effective minority carrier diffusion length [coupling the generation rates of mechanisms 4) and 5) in Fig. 1 into $G_{(4+5)}$].

For pulsed MOS capacitor measurements, the measured capacitance-time (C-t) data are converted into a Zerbst plot [i.e., $-d(C_{ox}/C)^2/dt$ versus $(C_f/C-1)$ plot] using the following equation [11]

$$-\frac{d(C_{ox}/C)^2}{dt} = \frac{2n_iC_{ox}}{\tau_{g,\text{eff}}N_AC_f}\left(\frac{C_f}{C}-1\right) + \frac{2K_{ox}n_is_{g,\text{eff}}}{K_st_{ox}N_A} \tag{2}$$

where

C_{ox}	oxide capacitance;
C_f	final (equilibrium) capacitance;
$\tau_{g,\text{eff}}$	effective generation lifetime;
$s_{g,\text{eff}}$	the effective surface generation velocity;
n_i	intrinsic carrier density;
N_A	boron density;
K_{ox} and K_s	dielectric constant for SiO_2 and Si, respectively.

The extrapolated intercept $(2K_{ox}n_is_{g,\text{eff}})/(K_st_{ox}N_A)$ of a Zerbst plot is a measure of the scr width-independent generation parameters, s_g', L_n and s_c in Fig. 1. These parameters, as described by the terms of $G_{(3)}$ and $G_{(4+5)}$ in (1), do not contribute to the current in space-charge region (I_{scr}). The slope $(2n_iC_{ox})/(\tau_{g,\text{eff}}N_AC_f)$ is related to the scr generation parameters, τ_g and s_g in Fig. 1. These parameters, as described by the terms of $G_{(1)}$ and $G_{(2)}$, contribute to I_{scr} which is given as

$$\begin{aligned} I_{\text{scr}} &= \frac{qn_iWA_G}{\tau_g} + qn_is_gA_S \\ &= \frac{qn_iWA_G}{\tau_g}\left(1+\frac{2s_g\tau_g}{r}\right) \\ &= \frac{qn_iWA_G}{\tau_{g,\text{eff}}} \end{aligned} \tag{3}$$

with

$$\begin{aligned} \tau_{g,\text{eff}} &= \left(\frac{1}{\tau_g}+\frac{1}{\tau_s}\right)^{-1} \\ &= \frac{\tau_g}{1+\tau_g/\tau_s} \end{aligned} \tag{4}$$

where

$\tau_{g,\text{eff}}$	effective generation lifetime in the space-charge region;
τ_g	bulk scr generation lifetime;
$\tau_s = (r/2s_g)$	lateral surface generation lifetime.

What is actually measured is a mixture of bulk scr and lateral surface generation lifetimes. In the limit of low surface generation velocity ($s_g \approx 0.1$–1 cm/s for well-passivated SiO_2/Si interfaces), the bulk scr lifetime τ_g dominates the surface lifetime τ_s (i. e., $\tau_s \gg \tau_g$ and $\tau_{g,\text{eff}} \approx \tau_g$) and the term of $(2s_g\tau_g/r)$ in e(3) becomes very small and is negligible. We can then rewrite (3) as

$$I_{\text{scr}} = \frac{qn_iWA_G}{\tau_g}. \tag{5}$$

B. Sample Preparation and Measurement Procedure

The test wafers were 5-in diameter, Czochralski-grown (CZ) p-type (100) silicon wafers with resistivity 10 Ω-cm. These wafers had an aluminum gate contact, 490 Å oxide thickness and a boron density of 1.25×10^{15} cm^{-3}. The iron density was determined by deep level transient spectroscopy (DLTS) measurements at room temperature to be 3.9×10^{12} cm^{-3}.

The pulsed MOS capacitor measurements were made with an MDC CSM/Win system. The system consists of: 1) a hot chuck probe station located within a dark box, 2) an HP 4284A (20 Hz to 1 MHz) Precision LCR meter with 0.01 fF resolution, 3) a temperature controller and 4) a water cooling system used for fast cooling the chuck. Capacitance measurements were carried out at a frequency of 100 kHz and a small ac signal of 40 mV. Fig. 2 is an outline of the Fe density detection procedure in this work.

Prior to the C-t measurements, the as-quenched sample was stored at room temperature (approximately 23 °C) for two weeks. This allowed a complete transformation of iron from Fe_i species to Fe–B pairs. The sample was initially biased into accumulation and then pulsed into deep depletion. The recovery time is determined by the thermal electron-hole pair (ehp) generation properties of the Si substrate and the Si/SiO_2 interface. A set of C-t data is measured. The wafer was then heated to 200 °C for 5 min, followed a by quenching to 23°C on a cold aluminum plate. Such a heat treatment dissociates the

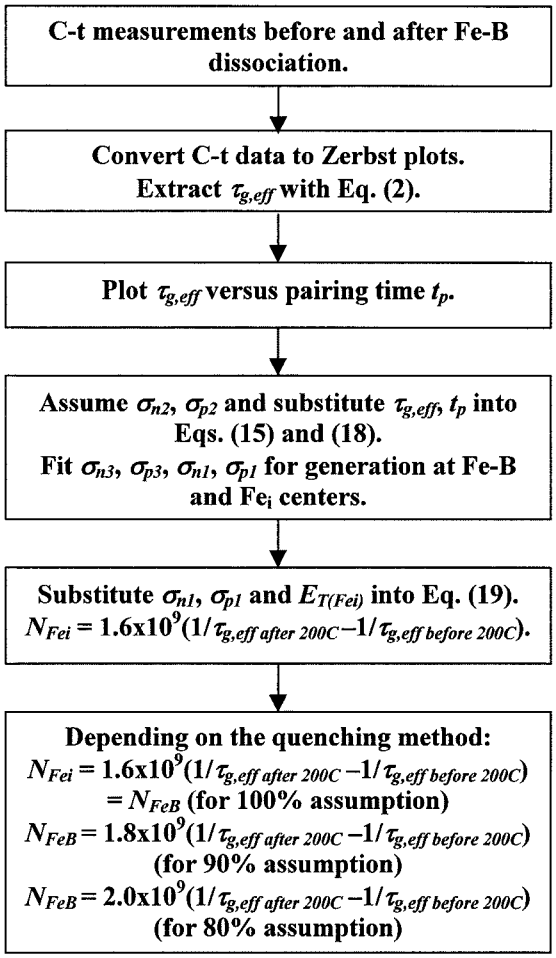

Fig. 2. Procedure to determine iron density by using the pulsed MOS capacitor generation lifetime measurement.

Fe–B pairs into interstitial iron (Fe_i) and substitutional boron (B), but does not lead to a permanent loss of Fe by precipitation [6]. During the process of Fe–B pair dissociation, C-t data were periodically measured. All C-t data measured before and after heating were converted into Zerbst plots using equation (2). The generation lifetimes were extracted from the slopes of the Zerbst plots. We will give more detailed discussion on this extraction method in Section IV.

III. Theoretical Background

Iron (Fe) can exist in one of the two states: either interstitial iron (Fe_i) or iron-boron pairs (Fe–B). Fig. 3 depicts the various energy levels of Fe_i and Fe–B in p-type silicon. Fe_i has an energy level at $E_v + 0.4$ eV (donor) [12], [13] whereas Fe–B pairs have two energy levels at $E_v + 0.1$ eV (donor) [12], [13] and $E_c - 0.29$ eV (acceptor) [13]–[15]. The presence of iron affects the generation lifetime [6], [16], [17]. Interstitial iron Fe_i with a deeper energy level is a more active generation site than Fe–B pairs.

Fe–B pairs are formed by Coulomb attraction and they dissociate at an elevated temperature, described by

$$(\mathrm{Fe^+B^-})^0 \leftrightarrow \mathrm{Fe}_i^+ + \mathrm{B}_s^-. \tag{6}$$

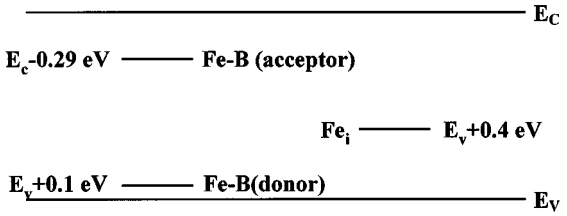

Fig. 3. The energy levels of Fe_i and Fe–B pairs in p-type silicon wafers.

Which of these state dominates depends on the temperature (T) and the boron density (N_A). At room temperature and boron densities greater than 10^{14} cm^{-3} [18], all iron forms pairs with boron as Fe–B. Upon heating at around 200 °C for boron densities less than 10^{16} cm^{-3}, most of the Fe–B pairs dissociate into Fe_i^+ and B_s^- [18]. As time elapses, interstitial iron Fe_i^+ reforms into Fe–B pairs with a time constant τ, given as [19]

$$\tau(m) = \frac{557T}{D_{\mathrm{Fe}_i} N_A}. \tag{7}$$

D_{Fe_i} is the diffusivity of the Fe_i^+ species [21], expressed as

$$D_{\mathrm{Fe}_i}(\mathrm{cm^2/s}) = 10^{-3} \times \exp[-0.67/(kT)] \tag{8}$$

with k as Boltzmann's constant. The high diffusivity of Fe in silicon is attributed to the difference in the elastic energies of the tetrahedral sites (T-sites) and hexagonal sites (H-sites) [21]. If $N_A = 1.25 \times 10^{15}$ cm^{-3} and $T = 296$K, then $\tau = 335$ min and $D_{\mathrm{Fe}_i} = 3.94 \times 10^{-13}$ cm^2/s according to (7) and (8).

The generation lifetime (τ_g), the time to generate one electron-hole pair (ehp) thermally, depends exponentially on the impurity energy level (E_T) and inversely on the capture cross sections of electrons (σ_n) and holes (σ_p). It is given as [22]

$$\begin{aligned}\tau_g &= \tau_n e^{-(E_T - E_i)/kT} + \tau_p e^{(E_T - E_i)/\mathrm{kT}} \\ &= \frac{e^{-(E_T - E_i)/kT}}{\sigma_n \nu_{th} N_T} + \frac{e^{(E_T - E_i)/kT}}{\sigma_p \nu_{th} N_T}\end{aligned} \tag{9}$$

where $\tau_n = (\sigma_n \nu_{th} N_T)^{-1}$ and $\tau_p = (\sigma_p \nu_{th} N_T)^{-1}$ are electron and hole lifetimes. ν_{th} is the thermal velocity, and N_T is the impurity density.

During the dissociation and reformation of Fe–B pairs after heating, the sum of Fe_i and Fe–B pair densities (N_T) remains unchanged at room temperature.

$$N_T = N_{\mathrm{Fe}_i}(t_p) + N_{\mathrm{FeB}}(t_p) \tag{10}$$

with $N_{\mathrm{Fe}i}(t_p)$ and $N_{\mathrm{FeB}}(t_p)$ as the densities of Fe_i and Fe–B at pairing time t_p after heating. The iron density of our test samples, as determined by DLTS measurements, is mainly attributed to Fe–B pairs before heating ($t_p = 0^-$). Assuming all Fe–B pairs totally dissociate into Fe_i immediately after heating ($t_p = 0^+$), we have

$$N_{\mathrm{FeB}}(t_p = 0^-) = N_T \tag{11}$$

$$N_{\mathrm{Fe}_i}(t_p = 0^+) = N_T. \tag{12}$$

Under the assumptions that all the interstitial iron atoms are ionized fully and the reformation of Fe_i species to Fe–B pairs obey

first-order reaction kinetics, the Fe_i density may be expressed as a function of pairing time t_p as

$$N_{Fe_i}(t_p) = N_{Fe_i}(t_p = 0^+)e^{-(t_p/\tau)} = N_T e^{-(t_p/\tau)} \quad (13)$$

where τ is the time constant of the Fe–B pairing reaction. Substituting (13) into (10), the Fe–B density at any given time t_p after thermal heating $N_{FeB}(t_p)$ can be expressed as

$$N_{FeB}(t_p) = N_T - N_{Fe_i}(t_p) = N_T - N_T e^{-(t_p/\tau)} = N_T(1 - e^{-(t_p/\tau)}). \quad (14)$$

Let τ_{g1}, τ_{g2} and τ_{g3} be the corresponding generation lifetimes of Fe_i at $E_v + 0.4$ eV and Fe–B pairs at $E_v + 0.1$ eV and $E_c - 0.29$ eV energy levels, respectively. From (9)–(14), we obtain

$$\tau_{g1} = \frac{e^{-(E_{T1}-E_i)/kT}}{\sigma_{n1}\nu_{th}N_T e^{-(t_p/\tau)}} + \frac{e^{(E_{T1}-E_i)/kT}}{\sigma_{p1}\nu_{th}N_T e^{-(t_p/\tau)}} \quad (15)$$

$$\tau_{g2} = \frac{e^{-(E_{T2}-E_i)/kT}}{\sigma_{n2}\nu_{th}N_T(1 - e^{-(t_p/\tau)})} + \frac{e^{(E_{T2}-E_i)/kT}}{\sigma_{p2}\nu_{th}N_T(1 - e^{-(t_p/\tau)})} \quad (16)$$

$$\tau_{g3} = \frac{e^{-(E_{T3}-E_i)/kT}}{\sigma_{n3}\nu_{th}N_T(1 - e^{-(t_p/\tau)})} + \frac{e^{(E_{T3}-E_i)/kT}}{\sigma_{p3}\nu_{th}N_T(1 - e^{-(t_p/\tau)})} \quad (17)$$

where E_{T1}, E_{T2} and E_{T3} are the corresponding impurity energy levels, σ_{n1}, σ_{n2}, σ_{n3}, σ_{p1}, σ_{p2} and σ_{p3} the corresponding electron and hole capture cross-sections. Thus, the total effective generation lifetime for Fe_i and Fe–B $\tau_{g,\text{eff}}$ becomes

$$\tau_{g,\text{eff}} = \left(\frac{1}{\tau_{g1}} + \frac{1}{\tau_{g2}} + \frac{1}{\tau_{g3}}\right)^{-1} \quad (18)$$

Fe_i with its energy level near the middle of the band gap is recognized as the most effective generation lifetime killer [4]–[6]. Under the assumption that hole ($\sigma_{p(Fei)}$) and electron ($\sigma_{n(Fei)}$) capture cross-sections of Fe_i do not differ too greatly (by a factor of 100 or less) [22], the Fe_i density immediately after 200°C heating can be described as [17]

$$N_{Fe_i}(\text{cm}^{-3}) = \frac{2}{\nu_{th}}\sqrt{\frac{1}{\sigma_{n(Fe_i)}\sigma_{p(Fe_i)}}}\cosh\left(\frac{E_{T(Fe_i)} - E_i}{kT}\right) \times \left(\frac{1}{\tau_{g,\text{eff}(after\ 200^\circ\text{C})}} - \frac{1}{\tau_{g,\text{eff}(before\ 200^\circ\text{C})}}\right) \quad (19)$$

with $E_{T(Fei)}$ as Fe_i impurity energy level, $\tau_{g,\text{eff}(before\ 200\ ^\circ\text{C})}$ and $\tau_{g,\text{eff}(after\ 200\ ^\circ\text{C})}$ the effective generation lifetimes before and after 200 °C heating.

IV. Results and Discussion

Fig. 4 is a plot of the measured C-t data for a boron-doped silicon MOS capacitor before and after heating at 200 °C for 5 min. During the C-t measurements, the device is initially biased into accumulation ($V_g = -3$ V) and then pulsed into deep depletion

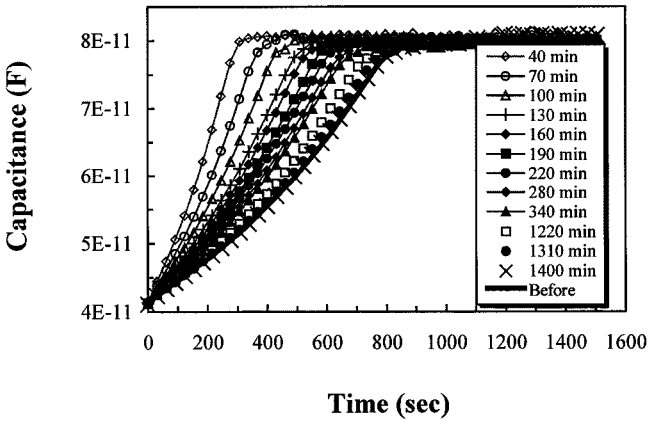

Fig. 4. C-t plots of an iron doped p-type silicon MOS capacitor before and after heating at 200 °C for 5 min.

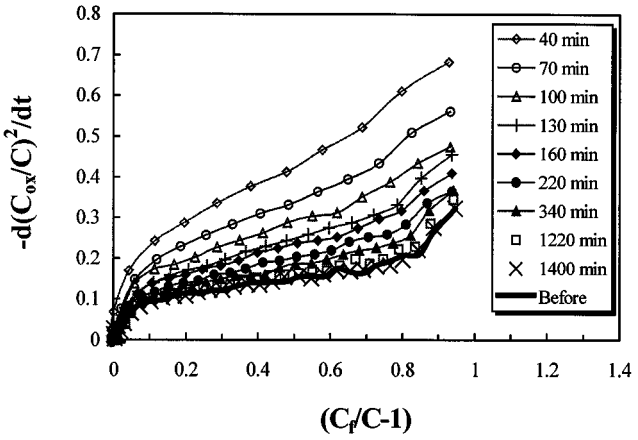

Fig. 5. Corresponding Zerbst plots of Fig. 4 obtained from (2).

($V_g = 3$ V). Thermal electron-hole pair generation returns the device to equilibrium over time. After about 1400 min pairing time t_p, the postheated C-t curve coincides with the preheated C-t curve, indicating reformation of all Fe_i into Fe–B pairs. This is approximately four times the time constant ($\tau = 335$ min) of the Fe–B pairing reaction, consistent with (13) and (14). Longer times do not change the C-t curve. Notice that the total C-t measuring time is kept far below the pairing time constant ($\tau = 335$ minutes) of the sample in this study.

Using (2), the corresponding Zerbst plots are obtained from the measured C-t data as illustrated in Fig. 5. The most useful part of these plots is the linear region. The portion near the origin is when the device approaches equilibrium. The curvature at the other end of the linear region has been ascribed to field-enhanced emission from interface and/or bulk traps [23], [24]. The postheated slope of the Zerbst plot decreases as pairing time t_p increases. At about 1400 min, the postheated line coincides with the preheated line and remains constant with time.

Effective generation lifetimes ($\tau_{g,\text{eff}}$) can be extracted from the slopes of the linear regions in Fig. 5 according to (2). Fig. 6 is a plot of $\tau_{g,\text{eff}}$ versus pairing time t_p. $\tau_{g,\text{eff}}$ is minimum immediately after heating when dissociation of Fe–B pairs occurs. As time elapses, $\tau_{g,\text{eff}}$ increases because Fe_i reforms into Fe–B pairs. The changes in $\tau_{g,\text{eff}}$ can be interpreted as follows. Due to the deep energy level of Fe_i ($E_v + 0.4$ eV), carriers are

TABLE I
VALUES OF ELECTRON AND HOLE CAPTURE CROSS-SECTIONS USED TO FIT THE DATA FOR RECOMBINATION (FALSTER *et al.* [27] AND ZOTH *et al.* [25]) AND GENERATION (THIS WORK) FOR Fe_i AND Fe–B CENTERS. ASSUMING $\sigma_{n2} = 5 \times 10^{-13}$ cm^2 $\sigma_{p2} = 10^{-15}$ cm^2 AND BY SUBSTITUTING ($\tau_{g,\text{eff}}$, t_p) DATA (ALL MEASURED AT T = 296 K AND OBTAINED FROM FIG. 6) INTO EQUATIONS (15)–(18), σ_{n1}, σ_{p1}, σ_{n3}, σ_{p3} CAN BE CALCULATED

	Recombination		Generation
	Falster *et al*. [27]	Zoth *et al*. [25]	This Work
Fe_i	E_v+0.38	E_v+0.38	E_v+0.4
σ_{n1} (cm^2)	5.5×10^{-14}	5.5×10^{-14}	4.6×10^{-14} (Calculation)
σ_{p1} (cm^2)	2.9×10^{-15}	1.5×10^{-15}	2.3×10^{-14} (Calculation)
FeB(+/o)	E_v+0.1	E_v+0.09	E_v+0.1
σ_{n2} (cm^2)	5×10^{-13}	5×10^{-13}	5×10^{-13} (Assumption)
σ_{p2} (cm^2)	1.8×10^{-13}	4.4×10^{-14}	1×10^{-15} (Assumption)
FeB(o/-)	E_c-0.28	E_c-0.29	E_c-0.29
σ_{n3} (cm^2)	5×10^{-13}	3×10^{-15}	4.5×10^{-13} (Calculation)
σ_{p3} (cm^2)	1.7×10^{-13}	3×10^{-15}	1.28×10^{-12} (Calculation)

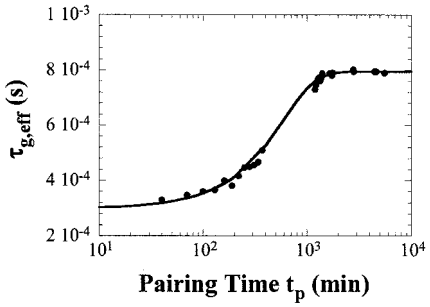

Fig. 6. Experimental (points extracted from Fig. 5) and calculated (solid line) generation lifetimes versus pairing time t_p after Fe–B pair dissociation.

readily generated immediately after the heating. In comparison, the Fe–B pairs have shallower energy levels. This gives rise to a relatively inefficient carrier generation and therefore a longer lifetime.

The experimental data ($\tau_{g,\text{eff}}$, t_p) can be well fitted with capture cross-sections for generation at Fe_i and Fe–B centers. Due to the shallow level, the Fe–B center at $E_v + 0.1$ eV is a less active generation site compared to the others (Fe–B at $E_C - 0.29$ eV and Fe_i at $E_v + 0.4$ eV). Its capture cross sections at room temperature (σ_{n2} and hole σ_{p2}) are approximately in the range of $10^{-13} \sim 10^{-15}$ cm^2 from the literature. Assuming $\sigma_{n2} = 5\times10^{-13}$ cm^2, $\sigma_{p2} = 10^{-15}$ cm^2 and by substituting ($\tau_{g,\text{eff}}$, t_p) data from Fig. 6, $E_i = 0.56$ eV, $E_{T1} = 0.4$ eV (Fe_i at $E_v + 0.4$ eV), $E_{T2} = 0.1$ eV (Fe–B at $E_v + 0.1$ eV), $E_{T3} = 0.83$ eV (Fe–B at $E_C - 0.29$ eV), $T = 296$K, $N_T = 3.9 \times 10^{12}$ cm^{-3} and $\tau = 335$ min [from equations (7) and (8)] into (15)–(18), the capture cross sections of Fe_i at $E_v + 0.4$ eV (σ_{n1}, σ_{p1}) and for Fe–B at E_C–0.29 eV (σ_{n3}, σ_{p3}) are obtained as given in Table I. Although there is some scatter in the experimental data, the general trend is that predicted by theory. Also shown in Table I is a list of capture cross-sections used to fit the data for recombination at Fe_i and Fe–B centers. These are values derived by Zoth *et al.* [25] from SPV measurements and a mixture of published data [6], [13], [26] as well as fitted values used by Falster *et al.* [27]. To check the effect of capture cross sections on generation lifetime, we used different combination of σ_n and σ_p for the curve fitting in Fig. 6. Three interesting observations are found from these curve fittings. First, assuming $\sigma_{n2} = 5\times10^{-13}$ cm^2 and $\sigma_{p2} = 10^{-15}$, the pre-heated effective generation lifetime $\tau_{g,before\ 200\text{C}}$ is sensitive to the hole capture cross section of the Fe–B 0.29 eV level (σ_{p3}) whereas the post-heated generation lifetime $\tau_{g,after\ 200\text{C}}$ is sensitive to the electron capture cross section of the Fe_i 0.4 eV level (σ_{n1}). Second, assuming $\sigma_{n2} = 5\times10^{-13}$ cm^2 and $\sigma_{p2} = 10^{-15}$, changes in σ_{n3} and σ_{p1} by a factor of 10 up or down hardly affect $\tau_{g,\text{eff}}$. Thirdly, changes in σ_{n2} and σ_{p2} (while σ_{n1}, σ_{p1}, σ_{n3}, σ_{p3} are constant, as given in Table I) by a factor of 10 up or down hardly affect $\tau_{g,\text{eff}}$. We point out here that capture cross sections measured under recombination and generation conditions may differ. Recombination takes place mainly in the quasineutral regions of a device or material with low or zero electric field. Generation, however, takes place in the space-charge region with significant electric field. Electric field influences the capture cross sections (capture cross section is a misnomer; it is really an emission cross section) during generation. Typically capture cross sections are reduced (i.e., emission cross sections are enhanced) in the presence of electric fields [23], [28]. An example of the capture cross section dependence on electric fields for metal impurities in silicon can be found in Tasch *et al.* [29]. In this case, the gold acceptor potential barrier is lowered in the presence of electric fields. This resulted in an increase of the thermal emission rate and a reduction in capture cross sections.

The rate of cooling after heating at 200 °C can affect the Fe–B dissociation. If the cooling rate is insufficiently fast, some of the dissociated Fe_i may reform into Fe–B pairs. Table II shows the influence of cooling rates on Fe–B pair dissociation by different quenching methods, as proven by DLTS and SPV measurements [6], [17]. In this work, our test sample was cooled quickly by quenching on a cold aluminum (Al) plate after thermal heating at 200 °C. Hence, we can assume the fraction of Fe_i left after quenching is approximately in the range of about 80–90%. In other words, only 80–90% of Fe–B pairs are activated to Fe_i after heating and quenching. The 20 to 10% loss of Fe_i will be taken into account in the analysis.

TABLE II
EFFECTS OF COOLING RATES ON Fe–B DISSOCIATION BY DIFFERENT QUENCHING METHODS AFTER THERMAL HEATING

Quenching methods	Cooling rates	Fraction of iron on interstitial sites	Loss of Fei by Fe-B pairing reaction
Water	Fast	100% [6]	0%
Al plate	Medium	90% [17]	10%
Al palte	Medium	80% [6]	20%
Air	Slow	50% [6]	50%

Substituting $\sigma_{n(\mathrm{Fei})} = 4.6 \times 10^{-14}$ cm^2, $\sigma_{p(\mathrm{Fei})} = 2.3 \times 10^{-14}$ cm^2, $E_{T(\mathrm{Fei})} = 0.4$ eV and $T = 296$K into equation (19), the Fe$_i$ density can be expressed as

$$N_{\mathrm{Fe}_i}(\mathrm{cm}^{-3}) = 1.6 \times 10^9 \times \left(\frac{1}{\tau_{g,\,\mathrm{eff}(after\ 200^\circ\mathrm{C})}} - \frac{1}{\tau_{g,\,\mathrm{eff}(before\ 200^\circ\mathrm{C})}} \right). \quad (20)$$

Assuming that 90% of the Fe–B is activated to Fe$_i$ after heating and quenching on a cold Al plate [17], the total Fe–B density in the space charge region is given as

$$N_{\mathrm{FeB}}(\mathrm{cm}^{-3}) = 1.8 \times 10^9 \times \left(\frac{1}{\tau_{g,\,\mathrm{eff}(after\ 200^\circ\mathrm{C})}} - \frac{1}{\tau_{g,\,\mathrm{eff}(before\ 200^\circ\mathrm{C})}} \right). \quad (21)$$

Similarly, under the assumption of 80% of Fe–B pairs activation to Fe$_i$ after heating and quenching [6], we obtain

$$N_{\mathrm{FeB}}(\mathrm{cm}^{-3}) = 2 \times 10^9 \times \left(\frac{1}{\tau_{g,\,\mathrm{eff}(after\ 200^\circ\mathrm{C})}} - \frac{1}{\tau_{g,\,\mathrm{eff}(before\ 200^\circ\mathrm{C})}} \right). \quad (22)$$

Substituting $\tau_{g,\,\mathrm{eff}(after\ 200^\circ\mathrm{C})} = 3 \times 10^{-4}$ s and $\tau_{g,\,\mathrm{eff}(before\ 200^\circ\mathrm{C})} = 7.95 \times 10^{-4}$ s (obtained from Fig. 6) into (21), (22) and (22), we find $N_{\mathrm{Fei}} = N_{\mathrm{FeB}} = 3.3 \times 10^{12}$ cm^{-3} (assumption: 100%), $N_{\mathrm{FeB}} = 3.7 \times 10^{12}$ cm^{-3} (assumption: 90%) and $N_{\mathrm{FeB}} = 4.2 \times 10^{12}$ cm^{-3} (assumption: 80%), respectively. These values are quite close to the iron density of 3.9×10^{12} cm^{-3} determined by DLTS measurements. Thus, equation (20) can be used to predict the iron density in p-type silicon wafers (with errors less than 15%). The constant of 1.6×10^9 depends on the aforementioned quenching methods. The important issue is that not only can the capture cross sections of Fe$_i$ used in equations (20)–(22) lead to reasonable expressions for N_{FeB} calculation, but they also fit the measured effective generation lifetimes $\tau_{g,\,\mathrm{eff}}$ in Fig. 6 very well. In other words, the constants of 1.6×10^9, 1.8×10^9 and 2×10^9 in equations (20)–(22) have been experimentally verified from both pulsed MOS generation lifetime and DLTS measurements. A linear dependence between $(1/\tau_{\mathrm{Fei}} - 1/\tau_{\mathrm{FeB}})$ and Fe$_i$ concentration (measured by SPV technique) was first reported by Walz *et al.* [30]. Obermeier *et al.* [17] reported this constant to be 8×10^8. The reason for the discrepancy from our measurements could be the difference in respective carrier capture cross sections for iron and iron–boron pairs. Apart from the capture cross sections, another parameter that affects the discrepancy in constants is the surface condition of the wafer under test. To achieve good iron detection precision, high quality samples with low surface generation velocity have to be used.

The detection limit of iron density depends strongly on the generation lifetime $\tau_{g,\,\mathrm{eff}(before\ 200\ ^\circ\mathrm{C})}$. Suppose $\tau_g/\tau_s = 2s_g\tau_g/r = 0.1$ and $s_g = 1$ cm/s in our test sample with $r = 0.5$ mm. According to equation (5), an effective generation lifetime $\tau_{g,\,\mathrm{eff}(before\ 200\ ^\circ\mathrm{C})}$ of 2500 μs is found. Assume the postheated generation lifetime to be 10% lower than the preheated generation lifetime, i.e., $\tau_{g,\,\mathrm{eff}(after\ 200\ ^\circ\mathrm{C})} \approx 0.9\tau_{g,\,\mathrm{eff}(before\ 200\ ^\circ\mathrm{C})}$. From equations (20)–(22), we obtain detection limits of about 2.2×10^{11} cm^{-3}, 2.5×10^{11} cm^{-3} and about 2.8×10^{11} cm^{-3} in this work. This limit is set by surface generation. For a surface with lower surface generation velocity, the detection limit is correspondingly reduced. The limit of about 10^{11} cm^{-3} shows good agreement with the experimental results reported by Kohno *et al.* [31]. In this case, the generation lifetimes were measured with the metal–insulator-semiconductor (MIS) and metal–air–insulator-semiconductor (MAIS) methods on a boron-doped Si before and after 210 °C heating. These experiments revealed that the generation lifetime reduced immediately after heating as Fe density was increased due to the dissociation of Fe–B pairs. Both methods were capable of detecting an iron density down to about 10^{11} cm^{-3}, consistent with the detection limit found in this work.

V. SUMMARY

The pulsed MOS capacitor generation lifetime technique can be used to determine the iron density in p-type silicon wafers. This technique is particularly suitable for measurements in thin layers. Upon heating at 200 °C for 5 min and quenching to 23°C, the effective generation lifetimes of boron-doped silicon MOS capacitor were extracted from the Zerbst plots before and after iron–boron (Fe–B) pair dissociation. An expression has been developed to determine the iron density. The constant of the N_{FeB} expression depends on the cooling rate after heating which varies with different quenching methods. An iron detection limit of about 10^{11} cm^{-3} was found in this work, consistent with the Kohno *et al.* [31]. The measurements in this work were made on conventional MOS capacitors. They can, of course, also be implemented by other space-charge region measurement techniques. For example, in one contactless method, the gate is held about 0.5 μm above the sample [31]–[33]. In another technique, the deep-depleted space-charge region is formed by a pulsed corona charge [34]. Equally valid are reverse-biased diode current measurements [11].

REFERENCES

[1] L. Jastrzebski, "An overview of effects of heavy metal contamination, wafer characteristics and gettering on device/circuit performance," in *Semiconductor Silicon*: Electrochem. Soc., 1990, pp. 614–627.
[2] K. Honda, T. Nakanishi, A. Ohsawa, and N. Toyokura, "Breakdown in silicon oxides (II)—Correlation with Fe precipitates," *Appl. Phys. Lett.*, vol. 46, pp. 582–584, Mar. 1985.

[3] B. O. Kolbesen and W. Pamler, "Surface and thin film analysis in silicon technology: Actual and future problems and demands," *Fresenius Z. Anal. Chem.*, vol. 333, pp. 561–568, 1989.
[4] T. S. Horanyi, P. Tutto, and C. Kovacsics, "Identification possibility of metallic impurities in p-type silicon by lifetime measurement," *J. Electrochem. Soc.*, vol. 143, pp. 216–220, Jan. 1996.
[5] A. Kempf *et al.*, "Influence of iron and copper on minority carrier recombination lifetime in silicon," in *Recombination Lifetime Measurements in Silicon*, D. C. Gupta, F. R. Bacher, and W. M. Hughes, Eds: Amer. Soc. Testing and Materials, 1998, vol. ASTM STP 1340, pp. 259–267.
[6] G. Zoth and W. Bergholz, "A fast, preparation-free method to detect iron in silicon," *J. Appl. Phys.*, vol. 67, pp. 6765–6771, June 1990.
[7] M. Zerbst, "Relaxation effects at semiconductor–insulator interfaces" (in German), *Z. Angew. Phys.*, vol. 22, pp. 30–33, May 1966.
[8] D. K. Schroder and H. C. Nathanson, "On the separation of bulk and surface components of lifetime using the pulsed MOS capacitor," *Solid-State Electron.*, vol. 13, pp. 577–582, July 1970.
[9] D. K. Schroder, "Bulk and optical generation parameters measured with the pulsed MOS capacior," *IEEE Trans. Electron Devices*, vol. ED-19, pp. 1018–1023, Sept. 1972.
[10] ——, "Effective lifetimes in high quality silicon devices," *Solid-State Electron.*, vol. 27, pp. 247–251, Mar. 1984.
[11] ——, *Semiconductor Material and Device Characterization*, 2nd ed. New York: Wiley, 1998, ch. 7.
[12] L. C. Kimerling and J. L. Benton, "Electronically controlled reactions of interstitial iron in silicon," *Physica B*, vol. 116, pp. 297–300, Feb. 1983.
[13] S. D. Brotherton, P. Bradley, and A. Grill, "Iron and the iron-boron complex in silicon," *J. Appl. Phys.*, vol. 57, pp. 1941–1943, Mar. 1985.
[14] Y. Hayamizu *et al.*, "Temperature dependence of minority-carrier lifetime in iron-diffused p-type silicon wafers," *J. Appl. Phys.*, vol. 69, pp. 3077–3081, Mar. 1991.
[15] A. Kaniava *et al.*, "Recombination activity of iron-related complexes in silicon studied by temperature dependent carrier lifetime measurements," *Appl. Phys. Lett.*, vol. 67, pp. 3930–3932, Dec. 1995.
[16] M. Miyazaki, M. Sano, S. Sumita, and N. Fujino, "Influence of metal impurities on leakage current of Si n^+p diode," *Jpn. J. Appl. Phys.*, vol. 30, pp. 295–297, Feb. 1991.
[17] G. Obermeier and D. Huber, "Iron detection in polished and epitaxial silicon wafers using generation lifetime measurements," *J. Appl. Phys.*, vol. 81, pp. 7345–7349, June 1997.
[18] H. Lemke, "Doping properties of iron in silicon" (in German), *Phys. Stat. Solids*, vol. A64, pp. 215–224, Mar. 1981.
[19] L. C. Kimerling, J. L. Benton, and J. J. Rubin, "Transition metal impurities in silicon," in *Defects and Radiation Effects in Semiconductors 1980*, ser. Inst. Phys. Conf. Ser. 59, 1981, pp. 217–222.
[20] S. A. McHugo *et al.*, "Iron solubility in highly boron-doped silicon," *Appl. Phys. Lett.*, vol. 73, pp. 1424–1426, Sept. 1998.
[21] A. A. Istratov, H. Hieslmair, and E. R. Weber, "Iron and its complexes in silicon," *J. Appl. Phys.*, vol. 69, pp. 13–44, Jan. 19899.
[22] D. K. Schroder, "The concept of generation and recombination lifetimes in semiconductors," *IEEE Trans. Electron Devices*, vol. ED-29, pp. 1336–1338, Aug. 1982.
[23] P. U. Calzolari, S. Graffi, and C. Morandi, "Field-enhanced carrier generation in MOS capacitors," *Solid-State Electron.*, vol. 17, pp. 1001–1011, Oct. 1974.
[24] K. S. Rabbani, "Investigations on field enhanced generation in semiconductors," *Solid-State Electron.*, vol. 30, pp. 607–613, June 1987.
[25] G. Zoth, "Aspects of silicon contamination control by lifetime measurements," in *Recombination Lifetime Measurements in Silicon*, D. C. Gupta, F. R. Bacher, and W. M. Hughes, Eds: Amer. Soc. Testing Mater., 1998, pp. 31–44.
[26] K. Graff and H. Pieper, "The behavior of transition and noble metals in silicon crystals," in *Semiconductor Silicon 1981*, H. R. Huff, R. J. Kriegler, and Y. Takeishi, Eds. Pennington, NJ: Electrochem. Soc., 1981, pp. 331–343.
[27] R. Falster and G. Borionetti, "The application of minority carrier lifetime techniques in modern CZ silicon," in *Recombination Lifetime Measurements in Silicon*, D. C. Gupta, F. R. Bacher, and W. M. Hughes, Eds: Amer. Soc. Test. Mater., 1998, pp. 226–249.
[28] J. Frenkel, "On the pre-breakdown phenomena in insulators and electronic semi-conductors," *Phys. Rev.*, vol. 54, pp. 647–648, Oct. 1938.
[29] A. F. Tasch Jr. and C. T. Sah, "Recombination-generation and optical properties of gold acceptor in silicon," *Phys. Rev. B*, vol. 1, pp. 800–809, Jan. 1970.
[30] D. Walz, J. P. Joly, and F. Tardif, "MOS generation lifetime for measuring metal contamination in silicon," in *Ultraclean Processing of Si Surfaces*, M. Heyns, Ed. Leuven, Belgium: Acco, 1994, pp. 139–142.
[31] M. Kohno *et al.*, "Noncontact measurement of generation lifetime," *Jpn. J. Appl. Phys.*, vol. 35, pp. 5539–5544, Oct. 1996.
[32] T. Sakai *et al.*, "Noncontact electrode-free capacitance/voltage measurement based on general theory of metal-oxide-semiconductor (MOS) structure," *Jpn. J. Appl. Phys.*, vol. 32, pp. 4005–4011, Sept. 1993.
[33] S. Hirae *et al.*, "Novel approach to evaluation of charging on semiconductor surface by noncontact, electrode-free capacitance/voltage measurement," *Jpn. J. Appl. Phys.*, vol. 33, pp. 1823–1830, Apr. 1994.
[34] D. K. Schroder *et al.*, "Corona-oxide-semiconductor device characterization," *Solid-State Electron.*, vol. 42, pp. 505–512, Apr. 1998.

Suat-Eng Tan was born in Johor, Malaysia. She received the B.S. degree from National Taiwan University, Taipei, Taiwan, R.O.C., and the Ph.D. degree from National University of Singapore, Singapore, both in electrical engineering, in 1993 and 1997, respectively. She conducted research on hot-carrier effects in submicron MOS devices during her Ph.D. study.

After she graduated, she joined the Department of Electrical Engineering, Arizona State University, Tempe, as a Post-Doctoral Researcher. During the summer of 1999, she was a Visiting Researcher at Mitsubishi Silicon America, OR. She is currently a Senior Process Integration Engineer at WaferTech, Camas, WA. Her current research interests include ULSI/VLSI device fabrication, defect studies, characterization and simulation of hot-carrier effects, and carrier lifetimes in semiconductor. She has published more than ten journal and conference papers in these fields.

Dieter K. Schroder (S'61–M'67–SM'78–F'86–LF'00) received his education at McGill University, Montreal, PQ, Canada, and at the University of Illinois, Urbana.

He joined Westinghouse Research Laboratories in 1968, where he was engaged in research on various aspects of semiconductor devices, including MOS devices, imaging arrays, power devices, and magnetostatic waves. He spent a year at the Institute of Applied Solid State Physics, Freiburg, Germany during 1978. In 1981 he joined the Center for Solid State Electronics Research, Arizona State University, Tempe. His current interests are semiconductor materials and devices, characterization, low power electronics, and defects in semiconductors. He is the author of *Advanced MOS Devices* and *Semiconductor Material and Device Characterization* and has published over 120 papers.

Motohiro Kohno was born in Japan, on May 14, 1957. He received the B.S. and M.S. degrees in electronics engineering from Hiroshima University, Hiroshima, Japan, in 1980 and 1982, respectively.

In 1984, he joined the Dainippon Screen MFG. Co. Ltd., Kyoto, Japan, where he has been engaged in research and development of noncontact *C–V* measurement technique. His current interests are noncontact techniques for in-line monitoring of contamination.

Mr. Kohno is a member of the Japan Society of Applied Physics.

Morimasa Miyazaki was born in Hyogo, Japan, in 1951. He received the B.E. degree from Osaka University of Education in 1974, the M.S. degree from Kyoto University in 1977, and the Ph.D. degree in electronic engineering from Okayama University in 1996.

In 1985, he joined Sumitomo Metal Industries, Saga, Japan, where he has been engaged in research of metal impurities and defects behavior in Si semiconductor material.

Dr. Miyazaki is a member of the Japan Society of Applied Physics.